ACS NANO
Cite This: ACS Nano XXXX, XXX, XXX−XXX
www.acsnano.org

ARTICLE

Air-Flow-Driven Triboelectric Nanogenerators for Self-Powered Real-Time Respiratory Monitoring

Meng Wang,[†] Jiahao Zhang,[†] Yingjie Tang,[†] Jun Li,[‡] Baosen Zhang,[†] Erjun Liang,[†] Yanchao Mao,*[,†] and Xudong Wang*[,‡]

[†]MOE Key Laboratory of Materials Physics, School of Physics and Engineering, Zhengzhou University, Zhengzhou 450001, China
[‡]Department of Materials Science and Engineering, University of Wisconsin−Madison, Madison, Wisconsin 53706, United States

Supporting Information

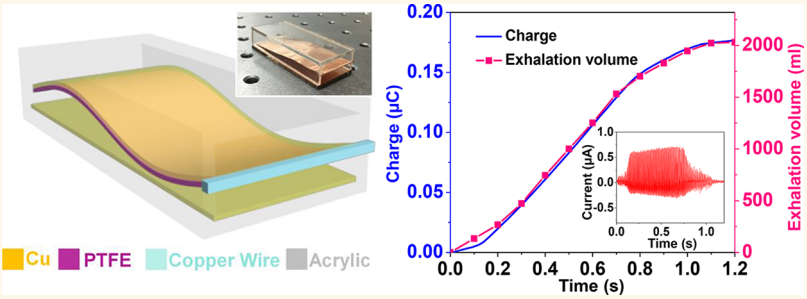

ABSTRACT: **Respiration is one of the most important vital signs of humans, and respiratory monitoring plays an important role in physical health management. A low-cost and convenient real-time respiratory monitoring system is extremely desirable. In this work, we demonstrated an air-flow-driven triboelectric nanogenerator (TENG) for self-powered real-time respiratory monitoring by converting mechanical energy of human respiration into electric output signals. The operation of the TENG was based on the air-flow-driven vibration of a flexible nanostructured polytetrafluoroethylene (n-PTFE) thin film in an acrylic tube. This TENG can generate distinct real-time electric signals when exposed to the air flow from different breath behaviors. It was also found that the accumulative charge transferred in breath sensing corresponds well to the total volume of air exchanged during the respiration process. Based on this TENG device, an intelligent wireless respiratory monitoring and alert system was further developed, which used the TENG signal to directly trigger a wireless alarm or dial a cell phone to provide timely alerts in response to breath behavior changes. This research offers a promising solution for developing self-powered real-time respiratory monitoring devices.**

KEYWORDS: *triboelectric nanogenerator, PTFE, mechanical energy harvesting, self-powered electronics, respiration monitoring*

Real-time biomonitoring has attracted tremendous attention in modern healthcare systems owing to the capability of instantaneously providing physical health status, early disease alert, and therapeutic treatments.[1−3] Such advanced systems have been applied to monitoring heart rate,[4] arterial pulse,[5] blood pressure,[6] and respiration.[7] Among them, respiration pattern is one of the most widely used human vital signs for personal health management. Current real-time respiratory monitoring devices are typically built on the principle of capacitive sensing, which are often associated with complex structure, large volume, and high cost, and thus are not very accessible for regular daily use.[8,9] In addition, like most other healthcare systems, these respiratory monitoring devices operate based on conventional batteries or external power sources, restricting their portability. Miniaturization and high-level user-friendliness are highly desired for next-generation real-time respiratory monitoring systems.

Triboelectric nanogenerators (TENGs), as an emerging technology for harvesting mechanical energy and generating electricity, have attracted great interest in recent years due to their portability, facile fabrication, low cost, and excellent adaptability.[10−14] The working mechanism of a TENG is based on the coupling of triboelectric friction and electric induction.[15] When two triboelectric materials with different electron-attracting abilities contact each other, surface charge transfer will be induced. The periodical contact and separation of the two charged surfaces will drive electron flow through an external circuit and produce electric output signals. In this regard, if air flow is used to induce harmonic vibration of a

Received: April 6, 2018
Accepted: May 30, 2018
Published: May 30, 2018

DOI: 10.1021/acsnano.8b02562
ACS Nano XXXX, XXX, XXX−XXX

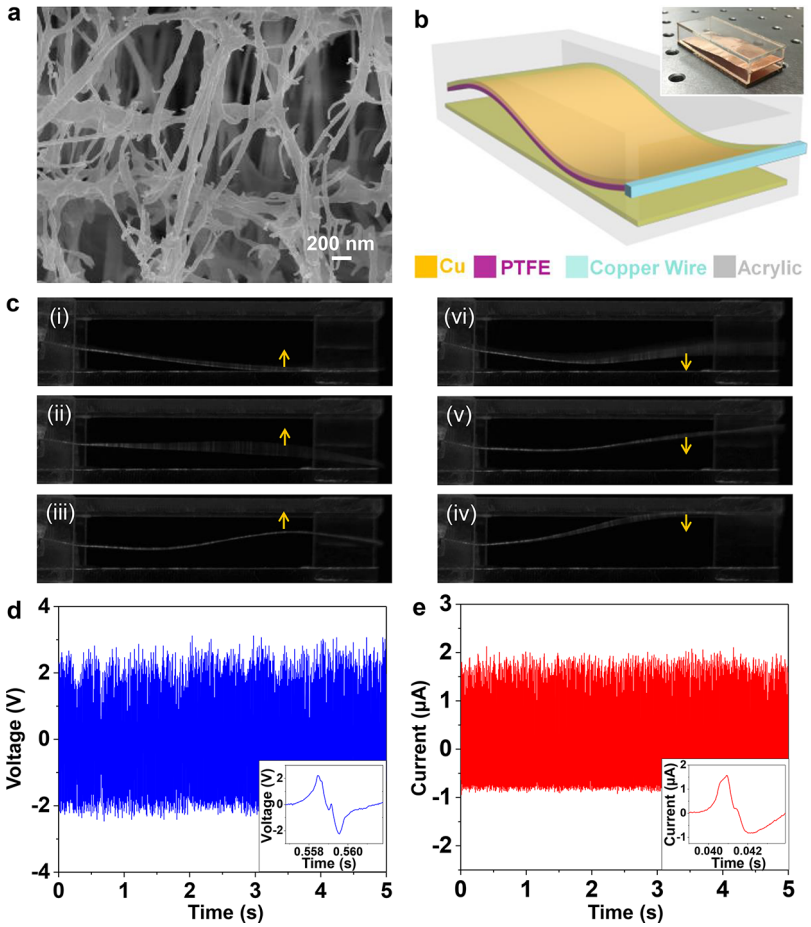

Figure 1. (a) SEM image of the n-PTFE thin film. (b) Schematic configuration of the air-flow-driven TENG. Inset shows a photograph of the TENG device. (c) Series of high-speed camera photos showing different vibration stages of an oscillating PTFE thin film in an acrylic tube. (d) Output voltage and (e) current signals recorded from the TENG at an air flow rate of 120 L/min. Insets depict the enlarged output signals during one oscillation cycle.

flexible triboelectric material and thus to create periodic contact/separation with another triboelectric material, mechanical energy from the air flow can be harvested and converted into electricity. Recent research has shown that using this configuration, TENGs were able to convert wind energy into electric energy for powering light-emitting diodes (LEDs).[16−19] In addition to serving as a power supply, the electricity from TENGs could also be directly processed as a responsive signal to realize self-powered sensing, such as pressure sensors,[20] vibration sensors,[21] speed sensors,[22] chemical sensors,[23] and body motion sensors.[24] Therefore, an air-flow-driven TENG shows promise for use in self-powered real-time respiratory monitoring. In this paper, we report the development of a flexible TENG that is driven by air flow from human respiration. The TENG was able to generate highly responsive electric signals corresponding to different breathing states and patterns. This TENG-based system thus provided a quantitative measure of breathing behavior without any additional power. By connecting it with a transmitter and signal processor, we also demonstrated a wireless data transmitting system enabling remote and real-time respiratory monitoring. This work demonstrated a promising solution for self-powered real-time respiratory monitoring as a highly portable and accessible healthcare module.

RESULTS AND DISCUSSION

The flexible TENG film was fabricated based on a nanostructured polytetrafluoroethylene (n-PTFE) thin film (Figure 1a) (fabrication details are included in the Experimental Section). The n-PTFE film is composed of a large number of nanofibers intertwined together, which yielded very high porosity and extremely large surfaces inside and on the surface of the PTFE film. The n-PTFE thin film offered a significantly enlarged contact area and surface area for charge transfer and induction, and thus was favorable for triboelectric electricity output. The high-porosity feature of the n-PTFE film also yielded a low film density and was desirable for flow-driven oscillation.[25] The design of the n-PTFE-based TENG is schematically shown in Figure 1b, and a photo of the device is shown in the inset. A very thin Cu film was attached onto the upper surface of the n-PTFE film for charge collection. One end of the n-PTFE film was affixed at the middle of an acrylic tube. The bottom surface of the acrylic tube was attached with another Cu electrode. When air flows into the acrylic tube, the PTFE thin film could be agitated to oscillate and make constant contact/separation with the bottom Cu electrode in the acrylic tube. The oscillation behavior of the n-PTFE/Cu film under an air flow rate of 120 L/min was captured using a high-speed camera, and the sequential images are shown in Figure 1c (the dynamic process can be seen in Video S1 in the Supporting Information). The oscillation frequency was ~120 Hz. No

DOI: 10.1021/acsnano.8b02562
ACS Nano XXXX, XXX, XXX−XXX

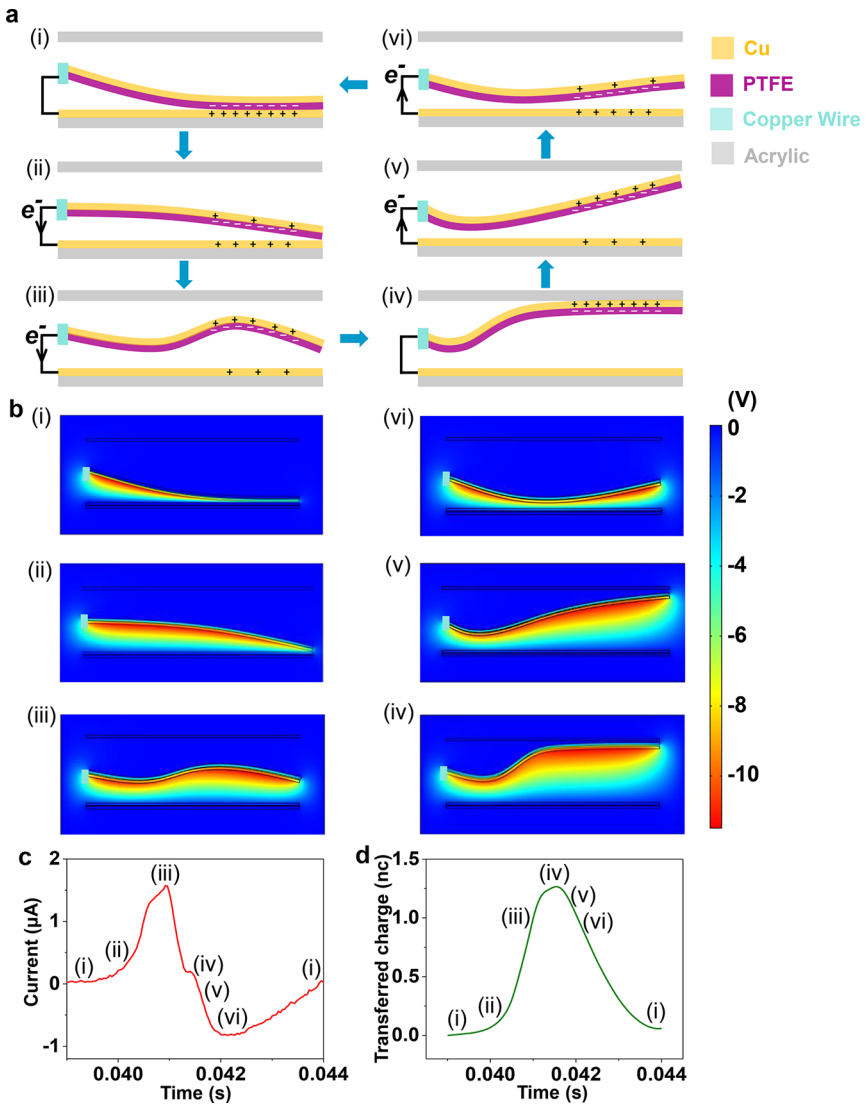

Figure 2. (a) Schematic diagrams showing the electricity generation process from the oscillating PTFE film inside the acrylic tube. (b) Corresponding electrical potential distribution simulated by the COMSOL software. (c) Output current signal generated from one oscillation cycle marked with different vibration stages. (d) Corresponding induced charge transfer calculated from the integral area of the *I*–*t* curve in (c).

adhesion was observed in the oscillation process, suggesting the excellent mechanical behavior of the n-PTFE/Cu film. It also confirmed the nonadhesive oscillations with minimal influences from the physical contact and charge transfer. Figure 1d and e illustrate the corresponding output voltage and current of the n-PTFE film. The average peak values of the output voltage and current reached 2.4 V and 1.7 μA, respectively. As shown in the insets of Figure 1d and e, the voltage and current output signals produced in one cycle exhibited a similar pattern. The short and nearly symmetric peak profiles further confirmed the excellent mechanical responses of the n-PTFE film with minimal hysteresis. The effective output performance of the TENG was further evaluated by connecting a series of loading resistors as external loads (Figure S1). The maximum output power of the TENG reached 1.3 mW at a load resistance of 15.1 MΩ.

The electricity generation process of the TENG was further analyzed in one cycle (Figure 2a). When the surfaces of the PTFE thin film and the bottom Cu electrode come in contact with each other, triboelectric charges will be generated due to the different triboelectric polarizations of PTFE and Cu.[26,27] Negative and positive electrostatic charges are thus generated on the surfaces of PTFE and Cu, respectively (step i). Once the air flow induces oscillation of the PTFE film, separation from the Cu electrode establishes an electric potential difference, which drives electrons flow from the back side of the PTFE thin film to the bottom Cu electrode through an external load, generating a positive output current (step ii). The current reaches the maximum at the largest separation point (step iii). When the negative charges on the PTFE thin film are fully compensated by the induced positive charges on its back side, current quickly drops back to zero (step iv). As the PTFE film moves back toward the bottom Cu electrode, the rising electric field drives electrons from the bottom Cu electrode to the back side of the PTFE film, producing a reverse output current signal in the external circuit (steps v, vi) until a new balance is established (step i). To support this proposed mechanism, corresponding electric potentials between the PTFE film and the bottom Cu electrode at the six steps were simulated using the COMSOL software (Figure 2b). The electric potential

DOI: 10.1021/acsnano.8b02562
ACS Nano XXXX, XXX, XXX–XXX

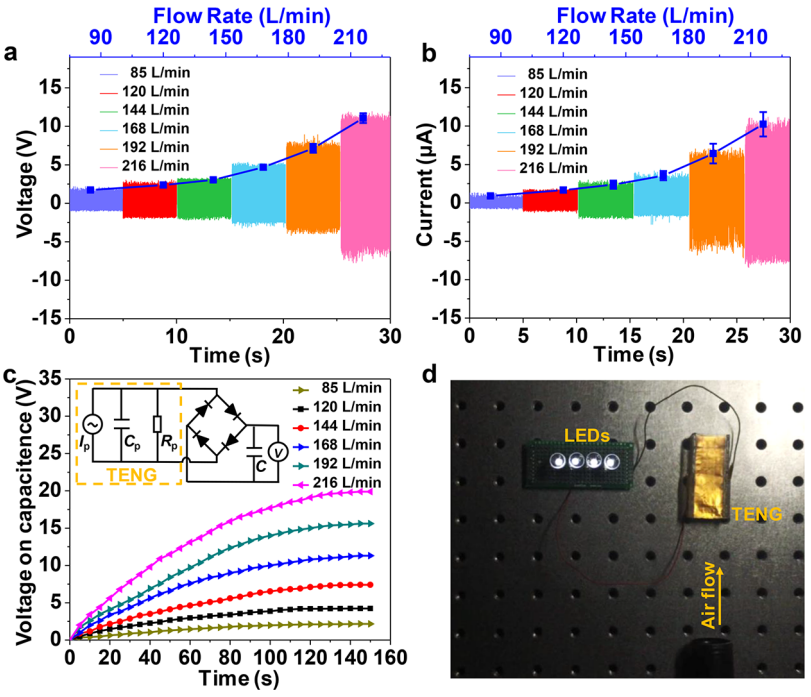

Figure 3. (a) Output voltage and (b) current signals recorded at different air flow rates ranging from 85 to 216 L/min. The corresponding average peak values are plotted as a function of flow rate, as depicted by the blue curves. (c) Charging processes of a 4.7 μF capacitor by the TENG under different air flow rates. Inset shows the equivalent circuit. (d) Four commercial white LEDs are lit by the TENG under an air flow rate of 120 L/min.

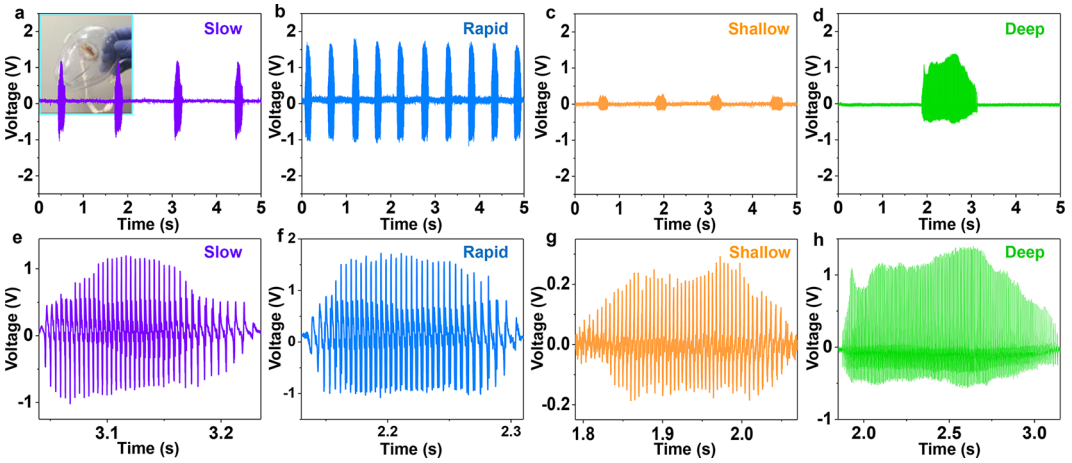

Figure 4. Real-time respiratory signals of the TENG, which were recorded from four different human breathing behaviors including (a) slow, (b) rapid, (c) shallow, and (d) deep breathing. Inset of (a) shows the TENG was embedded in a conventional medical mask for breath monitoring. (e–h) Corresponding enlarged voltage output envelop.

distribution was calculated under the ideal condition, *i.e.*, no external electron flow. It reveals the potential difference between the PTFE thin film and the bottom Cu electrode increased with their separation distance. Under the short circuit measurement condition, such potential differences will drive electron flow between the top and bottom Cu electrodes to neutralize the potential difference, generating an alternating current output in the external circuit. The recorded output current of a full contact–separation cycle is depicted in Figure 2c. Each step along the current pattern is marked accordingly in Figure 2a and b. The number of transferred charges was calculated by the integral area of the I–t curve in Figure 2c. As illustrated in Figure 2d, from point i to iv, the net charge transfer increased from 0 to 1.3 nC when the PTFE thin film was maximally contacting the bottom Cu electrode to a fully separated state. From point iv to vi, the net charge started decreasing, representing a backward charge flow. When maximal contact was reached again, the net charge dropped back to zero, suggesting the system reached its initial equilibrium stage.

The influence of air flow rate on the electrical output was then investigated. The output voltage and current measured from the TENG at different air flow rates are shown in Figure 3a and b, respectively. Both output voltages and currents exhibited fairly constant alternating values under a given air flow rate. The average peak values of output voltage and current rose monotonically from 1.7 V to 11.1 V and 0.9 μA to 10.2 μA, respectively, when the air flow rate increased from 85 L/min to

DOI: 10.1021/acsnano.8b02562
ACS Nano XXXX, XXX, XXX–XXX

216 L/min (Figure 3a and b). The air flow rate of 85 L/min is the U.S. standard required rate for the test of a respirator. The effect of humidity on the TENG performance was also investigated, as shown in Figure S2. When the relative humidity increased from 50% to 90%, the average peak values of output voltage and current decreased from 1.5 V to 0.4 V and 0.8 μA to 0.2 μA, respectively. This confirmed that the TENG would be able to deliver appropriate responses under highly humid conditions during normal human respiration. To demonstrate the capability as a power source, the air-flow-driven TENG was used to charge a commercial capacitor (4.7 μF) through a bridge circuit. The equivalent circuit for capacitor charging is given in the inset of Figure 3c. The alternating current (ac) output of the TENG was converted to a direct current (dc) output through the bridge circuit (Figure S3). The charging process of the capacitor under different air flow rates is shown in Figure 3c. It can be clearly seen that a higher air flow rate generated a higher saturation voltage of the capacitor, owing to the equilibrium between the capacitor leakage rate and charging rate of the TENG. The voltage held by the capacitor reached 19.9 V in 150 s under an air flow rate of 216 L/min. The electric energy generated by the TENG could directly light up four commercial white LEDs under an air flow rate of 120 L/min, as shown in Figure 3d and Video S2.

The highly sensitive responses of the n-PTFE TENG allowed direct generation of electricity in response to the air flow from human respiration. Such electric signals could be used as a real-time display of human respiration patterns. As a demonstration, the TENG was embedded in a conventional medical mask (inset of Figure 4a). When the mask was put on, normal breath would induce air flow through the acrylic channel where the n-PTEF TENG is installed and electric output would be generated accordingly. The working principle of the TENG for real-time monitoring of respiration is based on measuring the air flow of the exhalation process. This measurement method is the same as the standard pulmonary function test (PFT), which is generally used in current medical diagnosis. During the inhalation process, the flexible PTFE thin film was lying on the wall of the acrylic channel, leaving the half-channel open for air inlet to ensure minimal impact on inhalation. Therefore, our analysis was focused on the exhalation process. The electric signals were recorded under four different breathing patterns including slow, rapid, shallow, and deep breathing. As shown in Figure 4, it can be clearly seen that different breath patterns generated distinguishing electric output features. Slow breathing has a lower frequency, which is usually found in a calm and relaxed situation, such as sleep. It generated discrete groups of ac voltage peaks with a group width of 0.2 s (Figure 4a). The detailed feature of a voltage group is shown in Figure 4e. The voltage gradually peaked at 1.2 V in the middle of the envelop and then quickly dropped to 0.6 V in the final one-third of the period, matching well the slow breathing air flow pattern. Compared to slow breathing, rapid breathing has a higher rate. It generated more groups of voltage peaks than the slow breathing within the same time frame (Figure 4b). As shown in Figure 4f, the width of a peak group was also 0.2 s, while the voltage rapidly peaked at 1.8 V in the initial one-third of the period. Shallow breathing is usually found in a coma situation. It has a similar frequency to slow breathing but with a much shallower depth. The shallow breathing exhibited a weak voltage pattern with the peak value of 0.2 V and a similar group width of about 0.2 s, as shown in Figure 4c. The enlarged voltage group shown in Figure 4g revealed a slow increase of the peak voltage and a gradual drop after peaking at two-thirds of the envelop. Deep breathing had the longest breath period and the largest depth. Thus, it generated a more consistent high voltage output within one envelop of 1.3 s (Figure 4d). The detailed feature showed a rapid rise of the voltage at the beginning and a more steady high voltage in the initial two-thirds of the period. The distinct voltage envelop patterns allow direct recognition of human breath behavior, which is valuable for health situation monitoring.

In addition to distinguishing the breath patterns, the electric signals produced by the n-PTFE TENG could also be used to quantify the volume of air flow during breathing, which is another important vital sign for patients with respiratory disease, such as asthma and emphysema. Figure 5a shows the

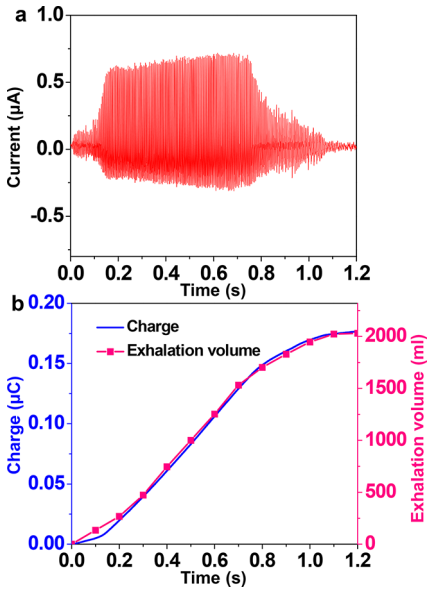

Figure 5. (a) Output current signal generated by one deep exhalation. (b) The blue curve is the amount of accumulative charge calculated by integrating the absolute area of the *I*−*t* curve. The pink curve is the volume of air transported during the exhalation process measured by an electric spirometer.

output current signal generated by one deep exhalation. The amount of accumulative charge was calculated by integrating the absolute area of the *I*−*t* curve. As shown by the blue curve in Figure 5b, the accumulative transferred charge gradually increased as a function of time and then reached a plateau of 0.18 C. The volume of air transported during the exhalation process was measured by an electric spirometer and plotted as a function of time (pink curve in Figure 5b). The accumulative charge and air volume exhibited a very good match along the entire time domain. This good match could be attributed to the high sensitivity of the TENG, which allowed it to be activated under a broad range of air flow rates. Therefore, the total amount of transferred charge detected by the TENG can provide a reliable measure of the volume of air exchanged during respiration.

On the basis of the advanced respiration monitoring capability, we further developed an intelligent wireless respiratory monitoring and alert system by integrating the n-PTFE TENG, a signal processing circuit, a wireless transmitter, an alarm, and a cell phone. In this system, the TENG could send an electric signal in response to different breath patterns

DOI: 10.1021/acsnano.8b02562
ACS Nano XXXX, XXX, XXX−XXX

without any additional power source. Once the breath pattern or volume reached a critical situation (*e.g.*, no breath for more than 5 s), an alarm was triggered through a wireless module and a warning massage was sent to the cell phone, providing timely alerts (Figures S4 and S5 and Videos S3 and S4). This demonstration showed the capability of using an n-PTFE TENG as a self-powered real-time respiratory monitoring device, which can provide electric signals readily integratable with comprehensive signal processing and communication systems.

CONCLUSIONS

In summary, we successfully developed an air-flow-driven TENG for self-powered real-time respiratory monitoring by converting the mechanical energy of human respiration into electric signals. The TENG was built on a flexible n-PTFE thin film, and the operation principle was based on the oscillation under laminar air flow. The n-PTFE TENG exhibited a sensitive electric signal output in response to different air flow rates. Therefore, when an n-PTFE TENG was installed in a regular mask, it was able to provide a real-time display of different breathing patterns. Integrating the total amount of charge transferred during one exhalation process showed an excellent match to the volume of air transported through the device, providing a quantitative measure of the breathing behavior. The real-time electric signal generated by this TENG device could be directly integrated with a wireless transmitter and signal processor, enabling an intelligent health monitoring system. This TENG device has a simple structure and is highly responsive to low-speed air flow. It opened opportunities for developing self-powered vital information monitoring systems.

EXPERIMENTAL SECTION

Fabrication of the TENG. The n-PTFE thin film was fabricated by using a biaxial stretching method. The PTFE powder (CD123, Asahi Fluoropolymers Co.) was mixed with the lubricant of 25 wt % naphtha. An extruder was used to extrude the mixture into a rod with a diameter of 13 mm. The rod was then rolled between two metal rollers into a sheet in air at 160 °C. The sheet was biaxially stretched at 170 °C with a constant rate, and then the stretched film was annealed in air at 330 °C. The n-PTFE thin film was obtained after cooling to room temperature. An acrylic tube with inner dimensions of 5.5 × 2 × 1 cm was made by a laser cutter. A piece of PTFE thin film was attached with a Cu foil to be one electrode. One end of the PTFE/Cu electrode was affixed onto the middle plane of the acrylic tube, resulting in the other end being free-standing. Another Cu electrode was fixed on the bottom surface of the acrylic tube.

Characterization and Measurement. The surface morphology of the PTFE thin film was characterized by a ZEISS Sigma 500 scanning electron microscope. An electric blower with adjustable speed was used to provide the air flow. The dynamic vibration process of the PTFE/Cu film was captured by a high-speed camera (BASLER aca1920). The output voltage and current of the TENG were measured by a Keithley 6514 system electrometer (1 MΩ internal resistant).

ASSOCIATED CONTENT

Supporting Information

The Supporting Information is available free of charge on the ACS Publications website at DOI: 10.1021/acsnano.8b02562.

Output voltage, current, and power *vs* different load resistances; the output voltage and current signals recorded under different relative humidity; the rectified output voltage; intelligent wireless respiratory monitoring and alert system; detailed circuit diagram of the SCM (PDF)

Air-flow-driven vibration behavior of the PTFE/Cu film captured using a high-speed camera (AVI)

Commercial white LEDs directly powered under an air flow rate of 120 L/min (AVI)

When a person stops breathing for more than 5 s, an alarm was wirelessly triggered through the respiratory monitoring and alert system (AVI)

When a person stops breathing for more than 5 s, a cell phone was dialed through the respiratory monitoring and alert system (AVI)

AUTHOR INFORMATION

Corresponding Authors

*E-mail: ymao@zzu.edu.cn.

*E-mail: xudong@engr.wisc.edu.

ORCID

Jun Li: 0000-0002-7498-6736

Xudong Wang: 0000-0002-9762-6792

Notes

The authors declare no competing financial interest.

ACKNOWLEDGMENTS

This work was supported by the National Natural Science Foundation of China (51503185), the National Institute of Biomedical Imaging and Bioengineering of the National Institutes of Health (R01EB021336), China Postdoctoral Science Foundation (2015M580636, 2016T90673), and Startup Research Fund of Zhengzhou University (1512317010).

REFERENCES

(1) Zheng, Q.; Shi, B.; Li, Z.; Wang, Z. L. Recent Progress on Piezoelectric and Triboelectric Energy Harvesters in Biomedical Systems. *Adv. Sci.* **2017**, *4*, 1700029.

(2) Zhang, Q.; Liang, Q.; Zhang, Z.; Kang, Z.; Liao, Q.; Ding, Y.; Ma, M.; Gao, F.; Zhao, X.; Zhang, Y. Electromagnetic Shielding Hybrid Nanogenerator for Health Monitoring and Protection. *Adv. Funct. Mater.* **2018**, *28*, 1703801.

(3) Park, D. Y.; Joe, D. J.; Kim, D. H.; Park, H.; Han, J. H.; Jeong, C. K.; Park, H.; Park, J. G.; Joung, B.; Lee, K. J. Self-Powered Real-Time Arterial Pulse Monitoring Using Ultrathin Epidermal Piezoelectric Sensors. *Adv. Mater.* **2017**, *29*, 1702308.

(4) Lin, Z.; Chen, J.; Li, X.; Zhou, Z.; Meng, K.; Wei, W.; Yang, J.; Wang, Z. L. Triboelectric Nanogenerator Enabled Body Sensor Network for Self-Powered Human Heart-Rate Monitoring. *ACS Nano* **2017**, *11*, 8830−8837.

(5) Kim, J.; Gutruf, P.; Chiarelli, A. M.; Heo, S. Y.; Cho, K.; Xie, Z.; Banks, A.; Han, S.; Jang, K. I.; Lee, J. W.; et al. Miniaturized Battery-Free Wireless Systems for Wearable Pulse Oximetry. *Adv. Funct. Mater.* **2017**, *27*, 1604373.

(6) Tricoli, A.; Nasiri, N.; De, S. Wearable and Miniaturized Sensor Technologies for and Personalized Preventive Medicine. *Adv. Funct. Mater.* **2017**, *27*, 1605271.

(7) Zhao, Z.; Yan, C.; Liu, Z.; Fu, X.; Peng, L. M.; Hu, Y.; Zheng, Z. Machine-Washable Textile Triboelectric Nanogenerators for Effective Human Respiratory Monitoring through Loom Weaving of Metallic Yarns. *Adv. Mater.* **2016**, *28*, 10267−10274.

(8) Liao, S. H.; Chen, W. J.; Lu, M. S. C. A CMOS MEMS Capacitive Flow Sensor for Respiratory Monitoring. *IEEE Sens. J.* **2013**, *13*, 1401−1402.

DOI: 10.1021/acsnano.8b02562
ACS Nano XXXX, XXX, XXX−XXX

(9) Hoffmann, T.; Eilebrecht, B.; Leonhardt, S. Respiratory Monitoring System on the Basis of Capacitive Textile Force Sensors. *IEEE Sens. J.* **2011**, *11*, 1112−1119.
(10) Fan, F. R.; Tian, Z. Q.; Wang, Z. L. Flexible Triboelectric Generator. *Nano Energy* **2012**, *1*, 328−334.
(11) Fan, F. R.; Lin, L.; Zhu, G.; Wu, W.; Zhang, R.; Wang, Z. L. Transparent Triboelectric Nanogenerators and Self-Powered Pressure Sensors Based on Micropatterned Plastic Films. *Nano Lett.* **2012**, *12*, 3109.
(12) Lai, Y. C.; Deng, J.; Zhang, S. L.; Niu, S.; Guo, H.; Wang, Z. L. Single-Thread-Based Wearable and Highly Stretchable Triboelectric Nanogenerators and Their Applications in Cloth-Based Self-Powered Human-Interactive and Biomedical Sensing. *Adv. Funct. Mater.* **2017**, *27*, 1604462.
(13) Mao, Y.; Zhang, N.; Tang, Y.; Wang, M.; Chao, M.; Liang, E. A Paper Triboelectric Nanogenerator for Self-Powered Electronic Systems. *Nanoscale* **2017**, *9*, 14499−14505.
(14) Wang, M.; Zhang, N.; Tang, Y.; Zhang, H.; Ning, C.; Tian, L.; Li, W.; Zhang, J.; Mao, Y.; Liang, E. Single-Electrode Triboelectric Nanogenerators Based on Sponge-Like Porous PTFE Thin Films for Mechanical Energy Harvesting and Self-Powered Electronics. *J. Mater. Chem. A* **2017**, *5*, 12252−12257.
(15) Mao, Y.; Geng, D.; Liang, E.; Wang, X. Single-Electrode Triboelectric Nanogenerator for Scavenging Friction Energy from Rolling Tires. *Nano Energy* **2015**, *15*, 227−234.
(16) Yang, Y.; Zhu, G.; Zhang, H.; Chen, J.; Zhong, X.; Lin, Z. H.; Su, Y.; Bai, P.; Wen, X.; Wang, Z. L. Triboelectric Nanogenerator for Harvesting Wind Energy and as Self-Powered Wind Vector Sensor System. *ACS Nano* **2013**, *7*, 9461−9468.
(17) Wang, X.; Wang, S.; Yang, Y.; Wang, Z. L. Hybridized Electromagnetic-Triboelectric Nanogenerator for Scavenging Air-Flow Energy to Sustainably Power Temperature Sensors. *ACS Nano* **2015**, *9*, 4553−62.
(18) Wang, S.; Mu, X.; Wang, X.; Gu, A. Y.; Wang, Z. L.; Yang, Y. Elasto-Aerodynamics-Driven Triboelectric Nanogenerator for Scavenging Air-Flow Energy. *ACS Nano* **2015**, *9*, 9554−63.
(19) Wang, J.; Zhang, H.; Xie, Y.; Yan, Z.; Yuan, Y.; Huang, L.; Cui, X.; Gao, M.; Su, Y.; Yang, W.; et al. Smart Network Node Based on Hybrid Nanogenerator for Self-Powered Multifunctional Sensing. *Nano Energy* **2017**, *33*, 418−426.
(20) Zou, J.; Zhang, M.; Huang, J.; Bian, J.; Jie, Y.; Willander, M.; Cao, X.; Wang, N.; Wang, Z. L. Coupled Supercapacitor and Triboelectric Nanogenerator Boost Biomimetic Pressure Sensor. *Adv. Energy. Mater.* **2018**, *8*, 1702671.
(21) Xu, M.; Wang, P.; Wang, Y. C.; Zhang, S. L.; Wang, A. C.; Zhang, C.; Wang, Z.; Pan, X.; Wang, Z. L. A Soft and Robust Spring Based Triboelectric Nanogenerator for Harvesting Arbitrary Directional Vibration Energy and Self-Powered Vibration Sensing. *Adv. Energy. Mater.* **2018**, *8*, 1702432.
(22) Xi, Y.; Guo, H.; Zi, Y.; Li, X.; Wang, J.; Deng, J.; Li, S.; Hu, C.; Cao, X.; Wang, Z. L. Multifunctional TENG for Blue Energy Scavenging and Self-Powered Wind-Speed Sensor. *Adv. Energy. Mater.* **2017**, *7*, 1602397.
(23) Wang, H.; Wu, H.; Hasan, D.; He, T.; Shi, Q.; Lee, C. Self-Powered Dual-Mode Amenity Sensor Based on the Water-Air Triboelectric Nanogenerator. *ACS Nano* **2017**, *11*, 10337−10346.
(24) Zhang, Q.; Liang, Q.; Liao, Q.; Yi, F.; Zheng, X.; Ma, M.; Gao, F.; Zhang, Y. Service Behavior of Multifunctional Triboelectric Nanogenerators. *Adv. Mater.* **2017**, *29*, 1606703.
(25) Sun, C.; Shi, J.; Wang, X. Fundamental Study of Mechanical Energy Harvesting Using Piezoelectric Nanostructures. *J. Appl. Phys.* **2010**, *108*, 034309.
(26) Cheng, G.; Zheng, H.; Yang, F.; Zhao, L.; Zheng, M.; Yang, J.; Qin, H.; Du, Z.; Wang, Z. L. Managing and Maximizing the Output Power of a Triboelectric Nanogenerator by Controlled Tip-Electrode Air-Discharging and Application for UV Sensing. *Nano Energy* **2018**, *44*, 208−216.
(27) Wang, J.; Wu, C.; Dai, Y.; Zhao, Z.; Wang, A.; Zhang, T.; Wang, Z. L. Achieving Ultrahigh Triboelectric Charge Density for Efficient Energy Harvesting. *Nat. Commun.* **2017**, *8*, 88.

DOI: 10.1021/acsnano.8b02562
ACS Nano XXXX, XXX, XXX−XXX